Spin-Orbit-Torque Switching in 20-nm Perpendicular Magnetic Tunnel Junctions

Mukund Bapna,[1] Brad Parks,[1] Samuel D. Oberdick,[1,2] Hamid Almasi,[3] Weigang Wang,[3] and Sara A. Majetich[1,*]

[1]*Physics Department, Carnegie Mellon University, Pittsburgh, Pennsylvania 15213, USA*
[2]*Applied Physics Division, Physical Measurement Laboratory, NIST, Boulder, Colorado 80305, USA*
[3]*Physics Department, University of Arizona, Tuscon, Arizona 85721, USA*

(Received 29 January 2018; revised manuscript received 4 June 2018; published 13 August 2018)

Magnetization switching utilizing the spin-orbit torque of heavy metals is a promising alternative to spin-transfer torque for a faster and more energy-efficient write mechanism for magnetic random-access memory. We report spin-orbit-torque switching in 20-nm-diameter $Co_{20}Fe_{60}B_{20}$-MgO-based perpendicular magnetic tunnel junctions with a thermal stability factor of ~47. Conductive atomic force microscopy was used to measure the tunnel magnetoresistance before and after current pulses through the heavy metal underlayer, and magnetostatic shifts in the minor loops provided evidence of spin-orbit-torque switching. Comparison of estimated critical current densities and write energies suggests that spin-orbit torque can be used as an effective switching mechanism for small and thermally stable perpendicular magnetic tunnel junctions.

DOI: 10.1103/PhysRevApplied.10.024013

I. INTRODUCTION

Magnetic memory, sensors, and microwave devices controlled with pure spin current or spin-orbit torque (SOT) have the potential for lower power dissipation and a longer lifetime than those based on spin-transfer torque (STT) [1,2]. Spin-polarized charge currents can switch a metallic nanomagnet [3], but high current densities are needed, and over time this can damage the thin tunnel barrier. Alternatively, when a charge current passes through a heavy metal conductor, a pure spin current j_s perpendicular to the charge current [4,5] leads to SOT on the adjacent magnetic layer [6,7] that can switch the magnetization direction [8,9]. Switching due to SOT has been detected through the Hall voltage or resistance [10–12] by spin-torque ferromagnetic resonance (ST-FMR) [8,13–15], by the magneto-optical Kerr effect (MOKE) [16,17], and by second-harmonic generation [18]. While proposed applications of SOT involve sub-100-nm magnets, the vast majority of these experiments have been performed on larger structures because the signals are small. For example, even when the magnetic material is several microns in diameter, the transverse spin Hall voltage is of the order of microvolts, and reducing the diameter reduces the magnitude of the signal. Many of the detection schemes require lock-in techniques, long averaging times, or angle-dependent measurements to distinguish the SOT contribution from other mechanisms [19]. Here the nanomagnet is part of a tunnel junction and the magnetoresistance is measured by conductive atomic force microscopy (cAFM), as shown in Fig. 1. cAFM is a point-contact technique that enables electrical measurement on the patterned devices at nanoscales. This technique eliminates the need for fabrication of smaller interconnects, which simplifies the overall patterning process flow for device testing at the prototype stage. We use cAFM for measurement of spin-current switching in small devices where size and surface-dependent effects may occur. For example, smaller current densities have been reported for reversal using STT in patterned films via coherent rotation in 20-nm devices than by nucleation plus domain-wall motion in larger devices [20]. Similar differences would be expected for reversal using SOT, but only the larger structures have been measured. To date no experimental demonstration of SOT switching for 20-nm, or smaller, perpendicular magnetic tunnel junctions (PMTJs) has been reported.

II. EXPERIMENTAL METHODS

The magnetic tunnel junction (MTJ) films in this study are deposited onto silicon wafers with 300 nm of thermal oxide in a 12-source UHV sputtering system. The deposition system is equipped with a residual gas analyzer for monitoring H_2O partial pressure and the base pressure is in the range of 10^{-9} Torr. The substrates are held at ambient temperature during deposition. The metallic layers are deposited by dc magnetron sputtering under an Ar pressure of 2 mTorr. The MgO layer is deposited by rf magnetron sputtering at 1.2 mTorr of Ar

[*]sara@cmu.edu

 © 2018 American Physical Society

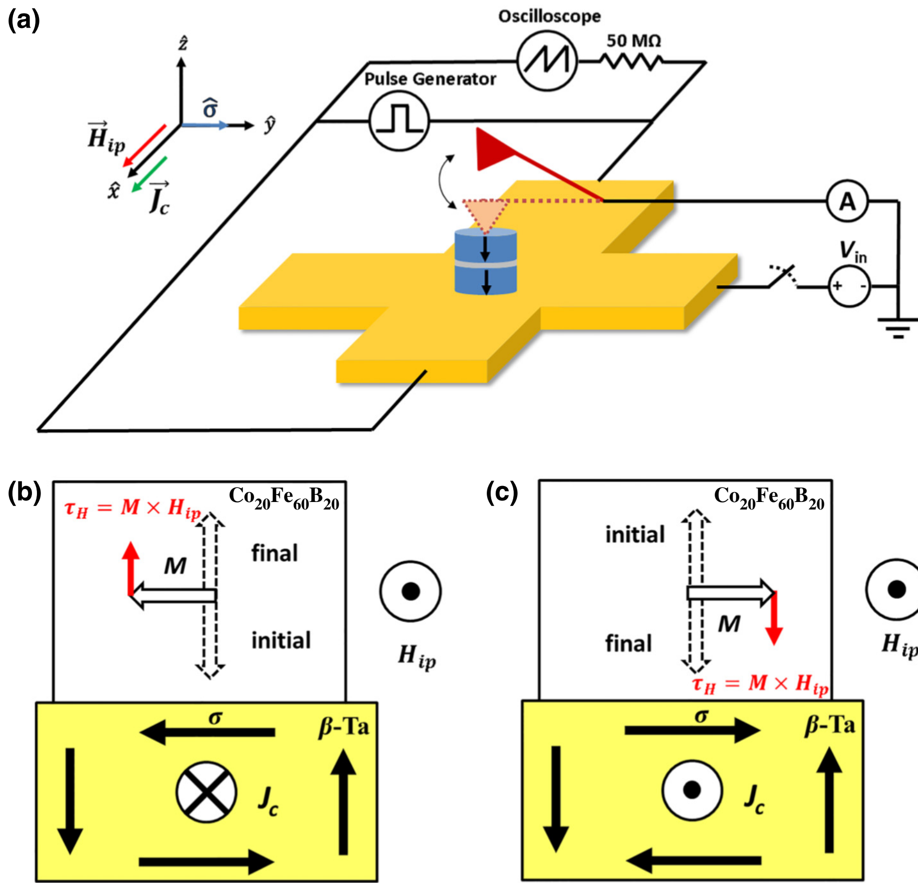

FIG. 1. Schematic of the experimental setup. A charge current pulse for SOT switching and detection of the MTJ resistance state using cAFM. A sharp conductive tip with an approximately 20-nm radius of curvature provides a point contact on top of the MTJ. TMR is measured to detect the state of the device, parallel (P) or antiparallel (AP). The tip is retracted (along $\hat{z}$) while a charge current pulse J_c (positive along $\hat{x}$) passes underneath the MTJ. The spin polarization $\hat{\sigma}$ provides torque along $\hat{y}$. The tip is brought in contact after the pulse to remeasure the TMR. The SOT pulls the magnetization in-plane and the fixed in-plane field H_{ip} determines the switching polarity as shown in (b),(c).

pressure. The structure of the MTJ stack is Ta(3)/Ru(5)/Ta(4)/$Co_{20}Fe_{60}B_{20}$(0.8)/MgO(1.5)/$Co_{20}Fe_{60}B_{20}$(1.5)/Ta(5)/Ru(9), where the numbers in parentheses are the film thicknesses in nanometers. The sample is annealed at 300 °C for 10 min. Samples are patterned into arrays of 20–200-nm MTJs at the intersections of Hall crosses with 8.7-μm-wide channels. The samples are then imaged by SEM to determine the MTJ diameters. The pillars are slightly tapered and the magnetic layers are near the bottom of the pillars. Details about the process flow can be found in the Supplemental Material [21].

A cAFM is then used to measure the resistance through the MTJ nanopillars as shown in Fig. 1. The instrument is an RHK UHV350 with R9 controller operating in contact mode, in air at 300 K. Si-doped AFM probe tips (Arrow-FM nanoworld) are made to be conducting by sputtering 200 nm (nominal thickness) of Pt on a Ta adhesion layer. The details of these point-contact measurements have been reported previously [22–24]. All cAFM measurements are made in air and at room temperature. In all resistance measurements through the MTJ, the tip is connected to ground and the voltage refers to the voltage at the base of the MTJ, where contact is made via one of the leads to the Hall cross. The tunnel magnetoresistance (TMR) as a function of magnetic field or bias is measured for individual MTJs using cAFM. A variable out-of-plane magnetic field H_{ext} up to 1300 Oe is applied by an electromagnet directly below the sample stage.

Symmetry breaking is required for SOT reversal of a perpendicularly magnetized layer [8,25], and so the sample is placed in the center of two permanent magnets to obtain a fixed in-plane magnetic field of 12.5 Oe along the charge current direction ($\hat{x}$) as is shown in Fig. 1. The effect of the SOT is to cant the magnetization towards the spin-polarization direction σ. When the magnetization points towards the spin-polarization direction, which is along the hard axis or the in-plane axis of the free layer, an external field is needed to break symmetry for deterministic switching as shown in Figs. 1(b) and 1(c). In the SOT switching experiments, cAFM is used to record the TMR as a function of field before and after current pulses through the Hall cross. In between, the tip is retracted by 100 nm in the $\hat{z}$ direction and the sample is isolated from the cAFM voltage source. This charge current is produced using a Global Specialties 4001 Ultravariable pulse generator, used in voltage-controlled and single-shot mode. The voltage is fixed at 8 V and the pulse width 200 μs, with rise and fall times less than 15 ns. An external oscilloscope (Tektronix model TDS 3032) with a 50 MΩ terminator is connected in parallel to the Hall cross to monitor the voltage drop.

This, together with the resistance measured by a multimeter (~200 Ω), is used to determine the charge current. After establishing the minimum charge current and pulse duration needed to observe SOT switching in the smallest devices, these parameters are kept constant for the remaining experiments. We then vary the current direction and the magnitude and direction ($\pm\hat{z}$) of the out-of-plane magnetic field. The perpendicular magnetic field is necessary both to initialize the MTJ in an antiparallel (AP) state and also to help in deterministic switching of the high-anisotropy bottom $Co_{20}Fe_{60}B_{20}$ layer using SOT.

III. RESULTS AND DISCUSSION

A. PMTJ imaging

Figure 2 shows three images of the sample: an optical image of the Pt leading to a β-Ta Hall cross, a SEM image of an array of MTJs within the Hall cross intersection, and a cAFM current map of the nanopillars.

Figure 2(c) shows the MTJ pillars when imaged by cAFM at low bias voltage, with $H = 0$. The color reflects the total amount of current passing from the Hall cross through to the cAFM tip. The background has virtually no current because the surface of the β-Ta has oxidized. For a constant resistance-area (RA) product, more current flows through a pillar with a larger diameter. The apparent size of the colored pillars is larger than the mentioned lateral sizes that are found using SEM imaging due to the large 200-nm tip radius of curvature of the wear-resistant tips used here for cAFM imaging. To make point contacts, and for electrical measurements, 20-nm MTJ cAFM tips with 20-nm tip radius of curvature were used. The RA product corresponding to the low resistance state measured at 10 mV was 6.2 Ω μm^2. We see uniform conductivity across individual devices. The apparently nonconducting regions seen in the conductivity map for larger devices are an artifact of residual resistance. Note that in several cases (100, 130, and 160 nm) there are two different current levels for devices of the same diameter. This arises because even without initialization some of the MTJs are in the parallel (P) state while others are in the AP state.

B. SOT switching of PMTJs

The applied field of the *in situ* electromagnet is not large enough to obtain major loops with reversal of both the top and bottom layers; therefore, an indirect method is used to determine the magnetization direction of the bottom $Co_{20}Fe_{60}B_{20}$ layer. This is achieved by measuring a minor loop for the top layer, where the loop shift (positive or negative) gives the direction of stray field (down or up) due to the bottom layer. If the top layer direction is unchanged, but SOT switches the bottom layer, the magnetostatic loop shift direction reverses.

Figure 3 illustrates how the current maps and minor loops change following SOT switching. Figure 3(a) shows an SEM image of the 20-nm device, and Figs. 3(b) and 3(c) show the current maps for the MTJ before and after the current pulse through the Ta underlayer. Minor loops of the resistance as a function of the applied magnetic field are also shown for the same 20-nm PMTJ, for two different directions of the bottom layer magnetization. A loop shift of 161 Oe is observed for this device size; similar observations were predicted in our previous work on magnetostatic effects in patterned PMTJs [23]. The method of using loop shifts to determine magnetization direction have also been previously utilized in magnetic multilayer systems [26,27]. In between the measurements shown in Figs. 3(d) and 3(e), a perpendicular field of +100 Oe is maintained, and a charge current pulse (200 μs, 40 mA) is passed through the heavy metal layers beneath the MTJ, switching the bottom layer. We do not observe any switching without the external out-of-plane field, suggesting that the torque due to the SOT alone is not sufficient to cause magnetization reversal at 40 mA. The role of the external out-of-plane field here is to reduce the required current density for SOT switching [28]. Once a switch is observed, checks are made to ensure it is not due to thermal activation. No switch is seen when initialized in the same AP state with the opposite current direction. However, switches are observed when both the bottom layer magnetization and the current direction are reversed. This is consistent with expectations for SOT switching, but not for thermally assisted switching, which would be random, or for an Oersted field from the

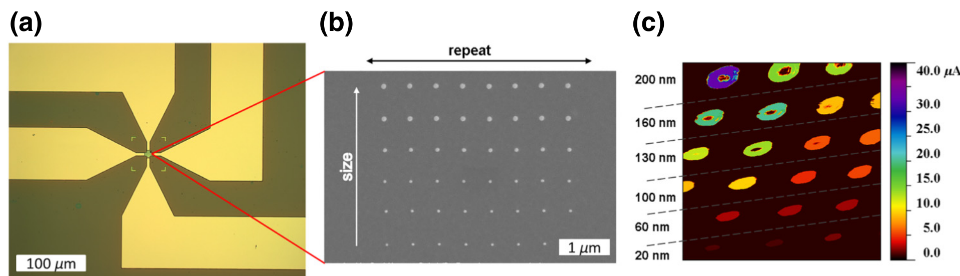

FIG. 2. (a) Optical image of photolithographically patterned Pt leading to a Hall cross. (b) SEM image of a MTJ array in one of the Hall crosses, with pillar diameters of 20, 60, 100, 130, 160, and 200 nm (bottom to top). The pillar height was 16 nm. (c) cAFM current map of the same nanopillars, taken at 20 mV bias. The sizes obtained from SEM are shown at the side. The scan size is 4×4 μm^2.

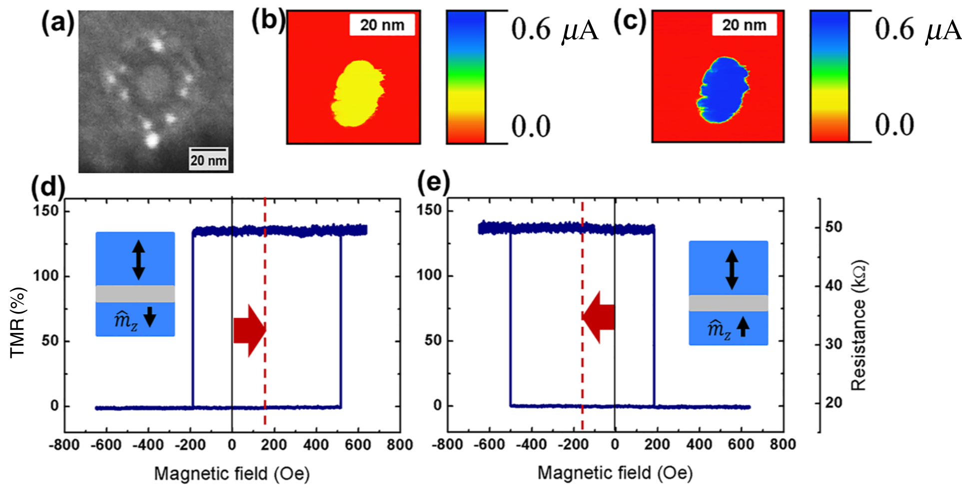

FIG. 3. (a) SEM image of a 20-nm device. Current maps measured using cAFM of the device initially in the AP state (b) and after SOT switching to the P state (c). Minor loop resistance for the 20-nm MTJ at 10 mV bias, showing different loop shift directions before (d) and after (e) the current pulse. The top layer coercivity is 353 Oe and the loop shift is 161 Oe.

current pulse, where switching would be independent of the current direction. These data illustrate two advantages of using a MTJ in SOT switching experiments. The TMR is 128% and resistance changes between 20 and 50 kΩ for the two states. Contrast this with Hall resistance measurements, where the typical differences range from mΩ to Ω, requiring lock-in techniques and angle-dependent measurements to differentiate SOT switching from other phenomena.

High current densities required to observe SOT switching are potentially troublesome for low-power applications of the SOT. In our switching experiments, the current amplitude is large because of the Ru layer below the Ta in the Hall cross base. The electrical resistivity of Ru ~7.6 $\mu\Omega$ cm [29,30] is, however, much smaller than for β-Ta ~190 $\mu\Omega$ cm [9], so the vast majority of the current flows through the Ru and contributes minimally to the SOT. Since Ru is a 4d metal and the strength of spin-orbit coupling scales as Z^4, Ru is expected to be far less efficient at transforming charge current to spin current than Ta. Moreover, the spin-diffusion length in Ru is less than 4 nm [31], and so Ru would act as a sink for spin current generated in the bottom Ta layer. Assuming uniform electrical contact through the bonding pad and ignoring oxidation, COMSOL simulations indicate a current density of 3.35×10^6 A/cm^2 in the top Ta layer and an additional 38% reduction in current density at the center of the cross, where the MTJs are located [21]. Similar reductions have been reported elsewhere [17]. The effective charge current density generating the spin current for switching is estimated to be $J_c^{\mathrm{SOT}} = 2.39 \times 10^6$A/cm^2, which is comparable to values typical of STT reversal, but without having to pass large current through the MTJ.

A second factor that impacts the SOT charge current amplitude is the high anisotropy of the adjacent $Co_{20}Fe_{60}B_{20}$ layer. Because major loops cannot be measured, the effective anisotropy $K_{\mathrm{eff,\,bottom}}$ is estimated indirectly. $K_{\mathrm{eff,\,top}}$ is found from switching field distributions of minor loops measured multiple times [21], and related to the interface anisotropy K_i, using a method that has been described previously [24]. The interface anisotropy K_i is determined from $K_i/t = K_{\mathrm{eff}} + |K_b| + |K_s|$, where t is the thickness. Thickness-dependent measurements on similar single-magnetic-layer films grown by the authors indicate $M_s = 1150$ emu/cm^3 and a reduced $K_b = 8.3$ erg/cm^3 [32]. With a top layer thickness of 1.5 nm, $K_i = 1.4$ erg/cm^2, and assuming the same K_i for the bottom layer, with thickness $t = 0.8$ nm leads to $K_{\mathrm{eff,\,bottom}} = 8.2$ erg/cm^3. The perpendicular magnetic anisotropy at the Fe/MgO interface is largely determined by the hybridization of Fe 3d orbitals and O 2p orbitals. In our MTJ stack with large TMR, careful control of the oxidation level results in the high K_{eff} value that we observe here [32,33]. If the bottom layer is considered as an isolated particle, its thermal stability factor $\Delta_{\mathrm{bottom}} = 47 \pm 2$ and the anisotropy field is $H_{\mathrm{eff,\,bottom}} = 14.3 \pm 1.3$ kOe.

C. Estimation of field-free critical current densities and write energies

The experiments reported here are done in a magnetic field, both to reduce the current requirements and to have deterministic switching, but by correcting for field effects it is possible to compare SOT and STT switching. The vast majority of the demonstrations of SOT switching are performed on MTJs with in-plane magnetization or a partial in-plane component. With PMTJs, a symmetry-breaking element is required for deterministic switching [17,34]. The SOT causes the out-of-plane magnetization to be pulled in-plane. Once the magnetization is in-plane, switching can then be achieved either stochastically by external perturbations such as thermal effects or deterministically by simultaneous application of an in-plane field. Deterministic switching can also be achieved through the STT effect [17,18]. STT-assisted SOT switching is

predicted to reduce the switching time and critical current density [17,34,35].

In our experiments an out-of-plane external field $H_{z,\mathrm{ext}} = 100$ Oe, far less than the anisotropy field $H_{\mathrm{eff,\ bottom}} = 14.3 \pm 1.3$ kOe, is used to demonstrate deterministic switching, but we can estimate the STT current that would be needed for field-free reversal. In a three-terminal device, the torque coming from STT would correspond to an additional current density $J_{\mathrm{add}}^{\mathrm{STT}} = (2e/\hbar)(\alpha\ t_f M_s/P)H_{z,\mathrm{ext}} = 6.64 \times 10^4 \mathrm{A/cm^2}$ through the device. Here e is the electron charge, $\hbar$ is Planck's constant, the damping parameter $\alpha = 0.015$ [36], the film thickness $t_f = 0.8$ nm, $M_s = 1150$ emu/cm^3 and the spin polarization factor $P = 0.62$, calculated using the Julliere formula $\mathrm{TMR} = 2P^2/(1-P^2)$ with $\mathrm{TMR} = 128\%$. In contrast, for a device with thermal stability $\Delta = 47$, the critical switching current density for pure STT switching is expected to be $J_{c0}^{\mathrm{STT}} = (2e/\hbar)(\alpha t_f M_s/\eta)H_{\mathrm{eff}} = 6.3 \times 10^6$ A/cm^2. In our case $(J_{\mathrm{add}}^{\mathrm{STT}} + J_c^{\mathrm{SOT}})/J_{c0}^{\mathrm{STT}} \approx 0.36$, suggesting that a reduction in the required current density is feasible using a STT-assisted SOT scheme.

We can also estimate the write energy per bit. From an application viewpoint, we assume an array of 20-nm devices, with 50-nm device-to-device distances on 4-nm-thick 50-nm-wide β-Ta channels. For SOT with deterministic switching, the switching time is estimated to be <10 ns [17,34]. As discussed above, switching can be achieved with $J_c^{\mathrm{SOT}} = 2.39 \times 10^6$ A/cm^2 through β-Ta with 190 $\mu\Omega$ cm resistivity and $J_{\mathrm{add}}^{\mathrm{STT}} = 6.64 \times 10^4$ A/cm^2 through a PMTJ with $R = 20$ kΩ. This yields energy consumption per switch in a cell $E_{sw}^{\mathrm{SOT+STT}} = \sum I^2 Rt \approx$ 0.1 fJ. Here the contribution due to the power dissipation from the STT current through the PMTJ is less than 10%. In contrast, the required energy per switch for the same cell using *only* STT current is estimated to be $E_{sw}^{\mathrm{STT}} \approx$ 0.3 pJ. Moreover, with STT switching the charge current passes through the high resistance MTJ, while with SOT switching it flows only through the heavy metal. When a charge current pulse travels through the Hall cross, all of the MTJs are exposed to the same spin current density. Hence multiple devices can be switched with the same voltage and current density, whereas such a scheme is impractical using STT due to high series resistance that the tunnel barriers would add. SOT could provide a dramatic reduction in energy consumption; however, challenges remain in fabricating such devices at scales where size-dependent effects may occur [21] and with proper interconnects to allow a three-terminal read and write.

IV. CONCLUSION

In summary, this work represents a very small and thermally stable perpendicular magnetic device switched using SOT, more than 300 times smaller in area than that in the pioneering demonstration of Miron *et al.* [8]. Our cAFM technique of switching detection based on TMR readout and magnetostatic loop shift is a simple way to detect switching in small devices with a large signal-to-noise ratio. The effective SOT charge current density through the Ta underlayer was less than that typical for STT reversal. Moreover, with field- or STT-assisted schemes such devices can be switched at much lower energy per write compared with the conventional STT scheme.

ACKNOWLEDGMENTS

This work was supported in part by STARnet, a Semiconductor Research Corporation project sponsored by MARCO and DARPA, under Contract No. 2013-MA-2831, and by NSF (Grant No. ECCS-1709845).

[1] A. Brataas, A. D. Kent, and H. Ohno, Current-induced torques in magnetic materials, Nat. Mater. **11**, 372 (2012).

[2] C. F. Pai, L. Liu, Y. Li, H. W. Tseng, D. C. Ralph, and R. A. Buhrman, Spin transfer torque devices utilizing the giant spin Hall effect of tungsten, Appl. Phys. Lett. **101**, 122404 (2012).

[3] J. Katine, F. Albert, R. Buhrman, E. Myers, and D. Ralph, Current-Driven Magnetization Reversal and Spin-Wave Excitations in Co/Cu/Co Pillars, Phys. Rev. Lett. **84**, 3149 (2000).

[4] E. Saitoh, M. Ueda, H. Miyajima, and G. Tatara, Conversion of spin current into charge current at room temperature, Inverse spin-Hall effect, Appl. Phys. Lett. **88**, 182509 (2006).

[5] K. Ando, S. Takahashi, K. Harii, K. Sasage, J. Ieda, S. Maekawa, and E. Saitoh, Electric Manipulation of Spin Relaxation using the Spin Hall Effect, Phys. Rev. Lett. **101**, 036601 (2008).

[6] M. I. D'yakonov and V. I. Perel, Possibility of orienting electron spins with current, JETP Lett. **13**, 467 (1971).

[7] J. E. Hirsch, Spin Hall Effect, Phys. Rev. Lett. **83**, 1834 (1999).

[8] I. M. Miron, K. Garello, G. Gaudin, P.-J. Zermatten, M. V. Costache, S. Auffret, S. Bandiera, B. Rodmacq, A. Schuhl, and P. Gambardella, Perpendicular switching of a single ferromagnetic layer induced by in-plane current injection, Nature **476**, 189 (2011).

[9] L. Liu, C.-F. Pai, Y. Li, H. W. Tseng, D. C. Ralph, and R. A. Buhrman, Spin-torque switching with the giant spin Hall effect of tantalum, Science (80) **336**, 555 (2012).

[10] Y. Kajiwara, K. Harii, S. Takahashi, J. Ohe, K. Uchida, M. Mizuguchi, H. Umezawa, H. Kawai, K. Ando, K. Takanashi, S. Maekawa, and E. Saitoh, Transmission of electrical signals by spin-wave interconversion in a magnetic insulator, Nature **464**, 262 (2010).

[11] K. Garello, I. M. Miron, C. O. Avci, F. Freimuth, Y. Mokrousov, S. Blügel, S. Auffret, O. Boulle, G. Gaudin, and P. Gambardella, Symmetry and magnitude of spin–orbit torques in ferromagnetic heterostructures, Nat. Nanotechnol. **8**, 587 (2013).

[12] C. Zhang, S. Fukami, H. Sato, F. Matsukura, and H. Ohno, Spin-orbit torque induced magnetization switching in nano-scale Ta/CoFeB/MgO, Appl. Phys. Lett. **107**, 12401 (2015).

[13] L. Liu, T. Moriyama, D. C. Ralph, and R. A. Buhrman, Spin-Torque Ferromagnetic Resonance Induced by the Spin Hall Effect, Phys. Rev. Lett. **106**, 036601 (2011).

[14] D. Fang, H. Kurebayashi, J. Wunderlich, K. Výborný, L. P. Zârbo, R. P. Campion, A. Casiraghi, B. L. Gallagher, T. Jungwirth, and A. J. Ferguson, Spin–orbit-driven ferromagnetic resonance, Nat. Nanotechnol. **6**, 413 (2011).

[15] S. I. Kiselev, J. C. Sankey, I. N. Krivorotov, N. C. Emley, R. J. Schoelkopf, R. A. Buhrman, and D. C. Ralph, Microwave oscillations of a nanomagnet driven by a spin-polarized current, Nature **425**, 380 (2003).

[16] G. Yu, P. Upadhyaya, K. L. Wong, W. Jiang, J. G. Alzate, J. Tang, P. K. Amiri, and K. L. Wang, Magnetization switching through spin-Hall-effect-induced chiral domain wall propagation, Phys. Rev. B **89**, 104421 (2014).

[17] A. van den Brink, G. Vermijs, A. Solignac, J. Koo, J. T. Kohlhepp, H. J. M. Swagten, and B. Koopmans, Field-free magnetization reversal by spin-Hall effect and exchange bias, Nat. Commun. **7**, 10854 (2016).

[18] A. Pattabi, Z. Gu, J. Gorchon, Y. Yang, J. Finley, O. J. Lee, H. A. Raziq, S. Salahuddin, and J. Bokor, Direct optical detection of current induced spin accumulation in metals by magnetization-induced second harmonic generation, Appl. Phys. Lett. **107**, 152404 (2015).

[19] J. Wunderlich, Current-switched magnetic insulator, Nat. Mater. **16**, 284 (2017).

[20] M. Gajek, J. J. Nowak, J. Z. Sun, P. L. Trouilloud, E. J. O'Sullivan, D. W. Abraham, M. C. Gaidis, G. Hu, S. Brown, Y. Zhu, R. P. Robertazzi, W. J. Gallagher, and D. C. Worledge, Spin torque switching of 20 nm magnetic tunnel junctions with perpendicular anisotropy, Appl. Phys. Lett. **100**, 132408 (2012).

[21] See Supplemental Material at http://link.aps.org/supplemental/10.1103/PhysRevApplied.10.024013 for details on Hall cross fabrication process flow, COMSOL simulations, switching field distributions, and variation of H_c and TMR with size.

[22] S. K. Piotrowski, M. F. Matty, and S. A. Majetich, Magnetic fluctuations in individual superparamagnetic particles, IEEE Trans. Magn. **50**, 2303704 (2014).

[23] M. Bapna, S. K. Piotrowski, S. D. Oberdick, M. Li, C.-L. Chien, and S. A. Majetich, Magnetostatic effects on switching in small magnetic tunnel junctions, Appl. Phys. Lett. **108**, 22406 (2016).

[24] S. K. Piotrowski, M. Bapna, S. D. Oberdick, S. A. Majetich, M. Li, C. L. Chien, R. Ahmed, and R. H. Victora, Size and voltage dependence of effective anisotropy in sub-100-nm perpendicular magnetic tunnel junctions, Phys. Rev. B Condens. Matter **94**, 14404 (2016).

[25] D. MacNeill, G. M. Stiehl, M. H. D. Guimaraes, R. A. Buhrman, J. Park, and D. C. Ralph, Control of spin–orbit torques through crystal symmetry in WTe2/ferromagnet bilayers, Nat. Phys. **13**, 300 (2016).

[26] V. Grolier, D. Renard, B. Bartenlian, P. Beauvillain, C. Chappert, C. Dupas, J. Ferré, M. Galtier, E. Kolb, M. Mulloy, J. P. Renard, and P. Veillet, Unambiguous Evidence of Oscillatory Magnetic Coupling between Co Layers in Ultrahigh Vacuum Grown Co/Au(111)/Co Trilayers, Phys. Rev. Lett. **71**, 3023 (1993).

[27] M. Matczak, L. Frackowiak, P. Kuswik, M. Urbaniak, B. Szymanski, and F. Stobiecki, Magnetization reversal and domain replication in Co–Au–Co film with perpendicular anisotropy, IEEE Trans. Magn. **50**, 1 (2014).

[28] L. Liu, O. J. Lee, T. J. Gudmundsen, D. C. Ralph, and R. A. Buhrman, Current-Induced Switching of Perpendicularly Magnetized Magnetic Layers Using Spin Torque from the Spin Hall Effect, Phys. Rev. Lett. **109**, 096602 (2012).

[29] S. Dutta, K. Sankaran, K. Moors, G. Pourtois, S. Van Elshocht, J. Bömmels, W. Vandervorst, Z. Tokei, and C. Adelmann, Thickness dependence of the resistivity of platinum-group metal thin films, J. Appl. Phys. **122**, 25107 (2017).

[30] J. W. Arblaster, Selected electrical resistivity values for the platinum group of metals part III: Ruthenium and osmium, Johnson Matthey Technol. Rev. **60**, 179 (2016).

[31] S. Yakata, Y. Ando, T. Miyazaki, and S. Mizukami, Temperature dependences of spin-diffusion lengths of Cu and Ru layers, Jpn. J. Appl. Phys. Part 1 Regul. Pap. Short Notes Rev. Pap. **45**, 3892 (2006).

[32] H. Almasi, C. L. Sun, X. Li, T. Newhouse-Illige, C. Bi, K. C. Price, S. Nahar, C. Grezes, Q. Hu, P. Khalili Amiri, K. L. Wang, P. M. Voyles, and W. G. Wang, Perpendicular magnetic tunnel junction with W seed and capping layers, J. Appl. Phys. **121**, 153902 (2017).

[33] H. Almasi, M. Xu, Y. Xu, T. Newhouse-Illige, and W. G. Wang, Effect of Mo insertion layers on the magnetoresistance and perpendicular magnetic anisotropy in Ta/CoFeB/MgO junctions, Appl. Phys. Lett. **109**, 32401 (2016).

[34] Z. Wang, W. Zhao, E. Deng, J.-O. Klein, and C. Chappert, Perpendicular-anisotropy magnetic tunnel junction switched by spin-Hall-assisted spin-transfer torque, J. Phys. D. Appl. Phys. **48**, 65001 (2015).

[35] K.-S. Lee, S.-W. Lee, B.-C. Min, and K.-J. Lee, Threshold current for switching of a perpendicular magnetic layer induced by spin Hall effect, Appl. Phys. Lett. **102**, 112410 (2013).

[36] T. Devolder, P. H. Ducrot, J. P. Adam, I. Barisic, N. Vernier, J. Kim, B. Ockert, and D. Ravelosona, Damping of Co x Fe 80-x B 20 ultrathin films with perpendicular magnetic anisotropy, Appl. Phys. Lett. **102**, 22407 (2013).